Sensitivity of Structurally Loaded Sandwich Panels to Localized Ballistic Penetration

Jørgen A. Kepler, Peter H. Bull

Sensitivity of Structurally Loaded Sandwich Panels to Localized Ballistic Penetration

Jørgen A. Kepler, Peter H. Bull

PII: S0266-3538(08)00094-8
DOI: 10.1016/j.compscitech.2008.03.005
Reference: CSTE 3996

To appear in: *Composites Science and Technology*

Received Date: 28 September 2007
Revised Date: 5 March 2008
Accepted Date: 6 March 2008

Please cite this article as: Kepler, J.A., Bull, P.H., Sensitivity of Structurally Loaded Sandwich Panels to Localized Ballistic Penetration, *Composites Science and Technology* (2008), doi: 10.1016/j.compscitech.2008.03.005

For ONR Special Issue

Sensitivity of Structurally Loaded Sandwich Panels to Localized Ballistic Penetration

Jørgen A. Kepler*, Peter H. Bull**

Department of Mechanical Engineering, Aalborg University, Denmark

*: Corresponding author, jk@ime.aau.dk

**: peb@ime.aau.dk

Abstract

This paper describes a series of tests focused on the combination of structural loading (bending, shear) and simultaneous penetrating impact on sandwich panels with thin GFRP face-sheets, with emphasis on the specific damage morphologies and developments depending on the type and magnitude of structural loading. The test specimens were sandwich panels, length 250 mm and width 150 mm, with carbon fibre prepreg face-sheets ([0°/90°], thickness $t_f \cong 0.5$ mm) bonded to the faces of a foam core (density 80 kg/m3, thickness H = 10 mm). The impact velocity was approximately 420 m/s, using a spherical steel impactor, diameter 10mm, with a mass of 4.1 g. A high-speed camera was used for registration of panel response. It was demonstrated, that, at preload levels above a specific limit, the impact would cause catastrophic failure, i.e. complete or near-complete loss of structural load carrying capacity. Developments of failure morphology, consistent with the observed evidence, were derived and outlined.

Keywords: sandwich, impact behaviour, damage mechanics, debonding, failure

1 Introduction

Sandwich panels, consisting of thin, rigid face-sheets bonded to the opposing sides of a thick, low-density core plate, are commonly used in structural applications where economy of material is critical. In an idealized representation of sandwich structures, external bending moments are balanced by opposing membrane forces in the face-sheets, while external transverse loads are balanced by transverse core shear. Consequentially, sandwich panels are normally designed for structural efficiency against bending deformation.

Generally, regardless of the actual structural element, the simultaneous combination of structural preload and localized impact is a potentially critical situation. Taken separately, the preload itself may be well within safety limits, and the puncture caused by a localized penetration without structural preload may be quite localized. In combination, however, the impact damage may initiate a damage process which eventually destroys the load carrying capacity of the structural component in question. Throughout this paper, such a process will be referred to as “catastrophic failure”.

Pressurized tubes, such as airplane fuselages and oil pipes, is a special case which has received some attention, see e.g. [1] by Rosenberg et al. In a recent study by Lu et al. [2], the “ballistic limit” of low-velocity impact on water-filled, pressurized metal pipes was studied. Mizukawa et al. [3] studied the static indentation and impact on thin-walled composite tubes, describing the typical failure pattern associated with a given combination of loading and tube geometry.

Sun and Chen [4] described force history and deflection of preloaded laminates under impact using a combined numerical and experimental approach. Zhang et al. [5] made an extensive study of composite laminate plates under compressive preload and impact, demonstrating the effect of preload level on the onset of catastrophic damage.

Similar combined loading on sandwich structures has apparently been largely neglected, despite the fact that sandwich structures, due to the high stiffness/weight-ratio, are

frequently used in transportation applications and so are susceptible to impact loads in general. A recent paper by Malekzadeh et al. [6] described a model for predicting the contact force and panel response when subjecting an in-plane prestressed sandwich panel to low velocity, nonpenetrating impact. It was, among other things, demonstrated that the peak contact force would increase and the deflection decrease with increasing tensile preload. However, the matters of overall structural response and possible catastrophic failure following penetrating impact were not addressed. A similar case for composite laminates was studied by Mitrevski et al. [7], who subjected test specimens to in-plane biaxial load and simultaneous transverse impact. A stiffening effect due to biaxial tension preload was observed, similarly to the results mentioned in [6], while damage sizes and absorbed energy was largely unaffected. Hertzberg and Weller studied a special case, impact on buckled composite panels, where an impact occurred on the convex or concave panel side, see [8]. Although the panels considered were not of sandwich type, the considerations of catastrophic damage and impact on convex or concave composite panels have a direct relation to the issues considered in the present paper.

In order to investigate the problem of potential catastrophic damage to sandwich panels, a number of tests were conducted. Sandwich specimens were subjected to symmetric or antisymmetric bending (corresponding to the aforementioned idealized situations) and local damage was caused by penetration of the specimen centre by a small-diameter steel impactor moving at high velocity.

2 Procedures and test specimens

Two structural preload cases were considered, symmetric and antisymmetric. While subjected to an appropriate preload level, the specimens were penetrated by a small, spherical steel impactor. The situations are outlined in Figure 1.

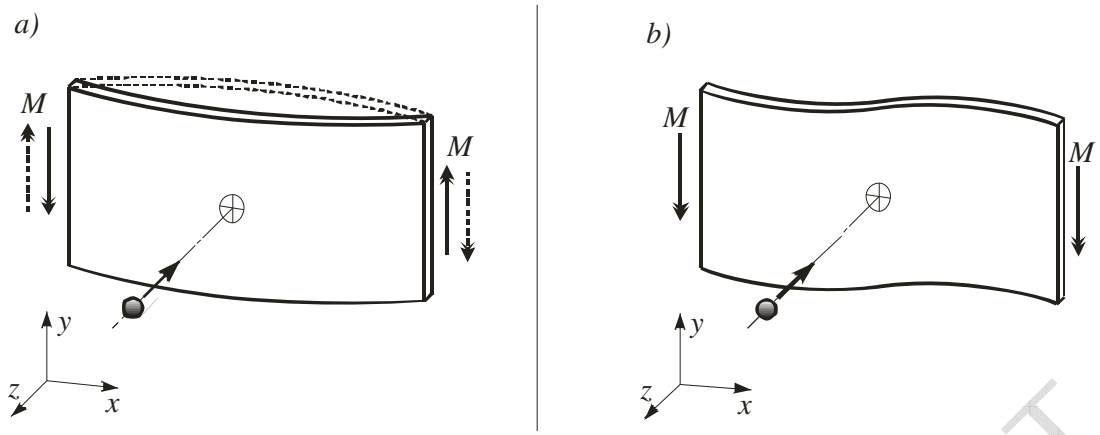

Fig. 1. Preload and impact scenarios. The panels were simply supported edges parallel to the y-direction edges and subjected to bending moment M along the supported edges.

Symmetric bending, as shown in Figure 1 a), introduces a constant bending moment along the specimen. Only the fully outlined case, with tension in the front face sheet, was considered. Antisymmetric bending, as outlined in Figure 1 b), ensures constant core shear stress along the specimen length.

A number of formally identical test specimens with a free specimen length of 250 mm and width 150 mm were manufactured. The material composition was:

- Lamina: UD prepreg, T700 carbon fibre with SE84LV epoxy resin, fibre mass 300 g/m^2, fibre volume fraction 60%, total mass 476 g/m^2, effective thickness 0.25 mm per lamina.
- Core: Polymethacrylimide (PMI) -foam, Rohacell 71 IG, thickness 10 mm
- Core end inserts: Mild steel, thickness 10 mm
- Sandwich layup [0°/90°/(core)/90°/0°], effective face-sheet thickness t_f = 0.50 mm (per face-sheet, verified by microscopy).

The steel core inserts were used as core material at the preload application ends. The test specimen geometry is shown in Figure 2. For the symmetric bending tests, the

compressed face-sheets were reinforced in the transition zone between steel core inserts and foam core.

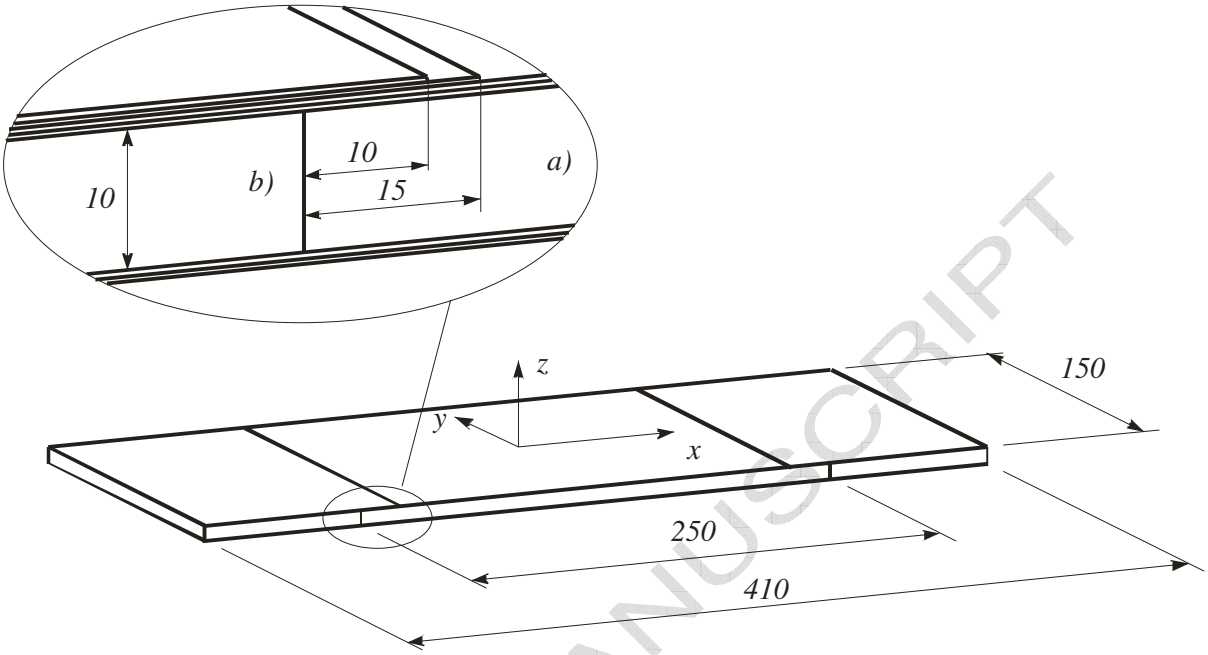

Fig. 2. Specimen geometry. All dimensions in mm. The specimens were symmetric about the yz-plane. The magnified view shows the local reinforcement of the compressed face sheet ([0°/90°/0°/90°] dropping to [90°/0°/90°] dropping to [0°/90°]) in the transition zone between steel core (b) and foam core (a).

The specimens were manufactured in three stages:

- Steel core inserts and foam core were bonded, using a 2-component epoxy adhesive, and left to cure for several days.
- [0°/90°] face-sheet plies were applied and cured in a vacuum bag at elevated temperature, as outlined in the appropriate data-sheet.
- Reinforcement plies added on compressive side face-sheet, cured as primary plies.

The structural preloads were applied to the steel-insert end zones of the specimens . The free-body diagrams in Figure 3 indicate the resulting moment and shear distributions.

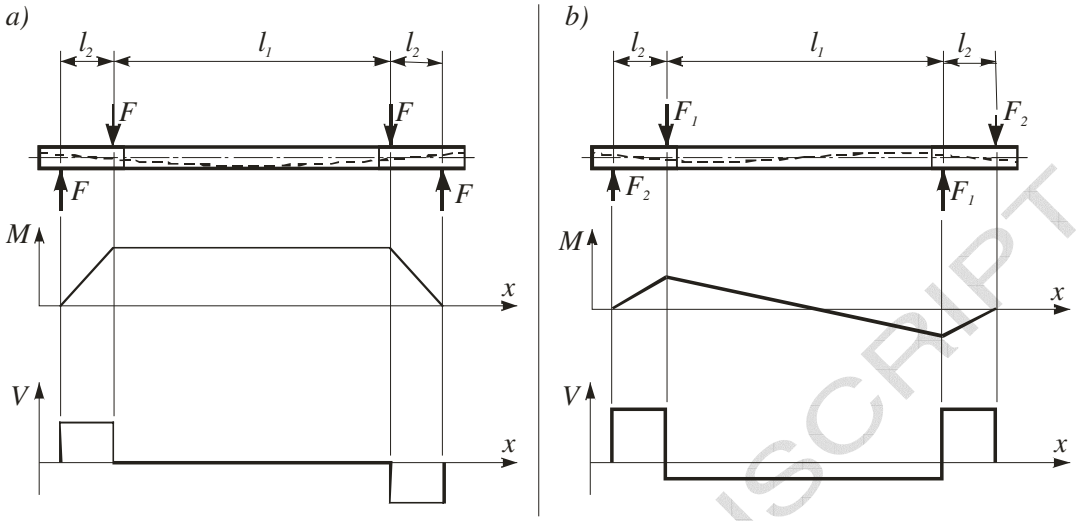

Fig. 3. Free-body diagrams with corresponding moment distribution M and shear force distribution V for symmetric bending (a) and antisymmetric bending (b). The dashed line indicates specimen deformation.

As seen in Figure 3, the load conditions introduce

3 a) Moment M constant, and shear V = 0, along the free specimen length.

3 b) Shear V constant along the free specimen length, and moment M = 0 at the specimen centre

3 Static tests

For determining the maximum feasible preload level, a number of specimens were tested to failure in a quasi-static test setup (without impact). The test setup, essentially a wide-specimen 4-point beam bending test, is outlined in Figure 4 (shown for symmetric bending).

Fig. 4: Static test setup.

Due to the diameter and relative proximity of the rollers, it was necessary to compensate for geometric nonlinearity. Figure 5 outlines the geometric factors for compensation, shown for the right end of the test specimen.

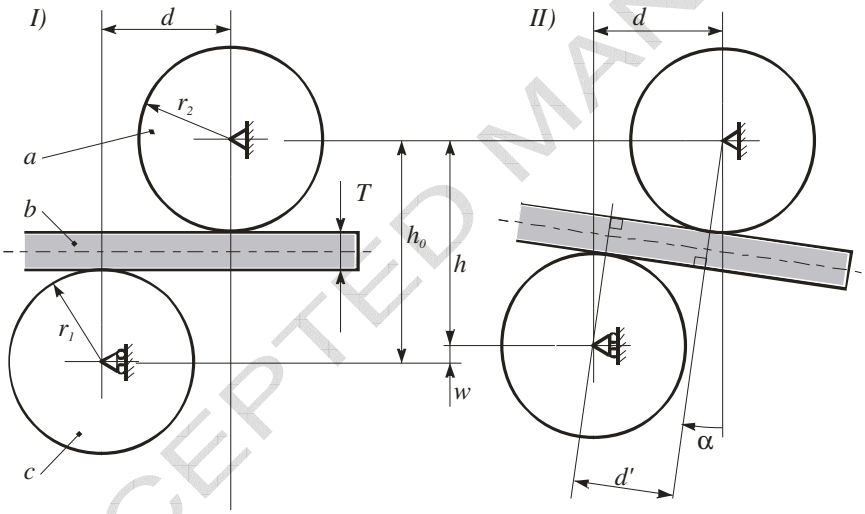

Fig. 5: Nonlinear development of contact distance from d in the undeformed state (I) to d' at moderate angles α (II).

a: top roller, b: specimen (right end), c: bottom roller.

In figure 5, w is the measured crosshead displacement. The horizontal distance d remains constant, while the contact point distance d' = d'(w). Similar geometric

corrections apply to the measured crosshead force to obtain the perpendicular force at the contact points.

3.1 Static symmetric bending. On the specimens subjected to symmetric bending (Figure 3 a), strain gauges were bonded to the face sheets to provide a measurement of the preload-induced strain in the x-direction. 3 specimens were tested, giving an average ultimate preload ε_{ult} = 4400 μstrain. All three specimens failed by compressive face-sheet failure in the transition zone between steel and foam core, indicating a moderate amount of local face-sheet bending.

3.2 Static antisymmetric bending. Two specimens were subjected to antisymmetric bending (Figure 3 b) and failed at an average equivalent ultimate core shear stress of τ_{ult} = 1.18 MPa. The failure mode was core fracture at an angle of 45° relative to the specimen midplane. The core material manufacturer indicates an ultimate core shear stress of 1.30 MPa.

4 Test setups for combined preload and impact

The tests with simultaneous structural preload and impact were conducted using a combination of gas gun, preload frame and high-speed camera.

The impactor, a 10mm steel sphere, mass 4.1 g, would in all tests impact the specimen at a velocity of 415-420 m/s (substantially higher than the ballistic limit), causing full penetration.

The test setups for the two different types of preload (symmetric – constant bending moment, and antisymmetric – constant shear force) are shown in Figure 6.

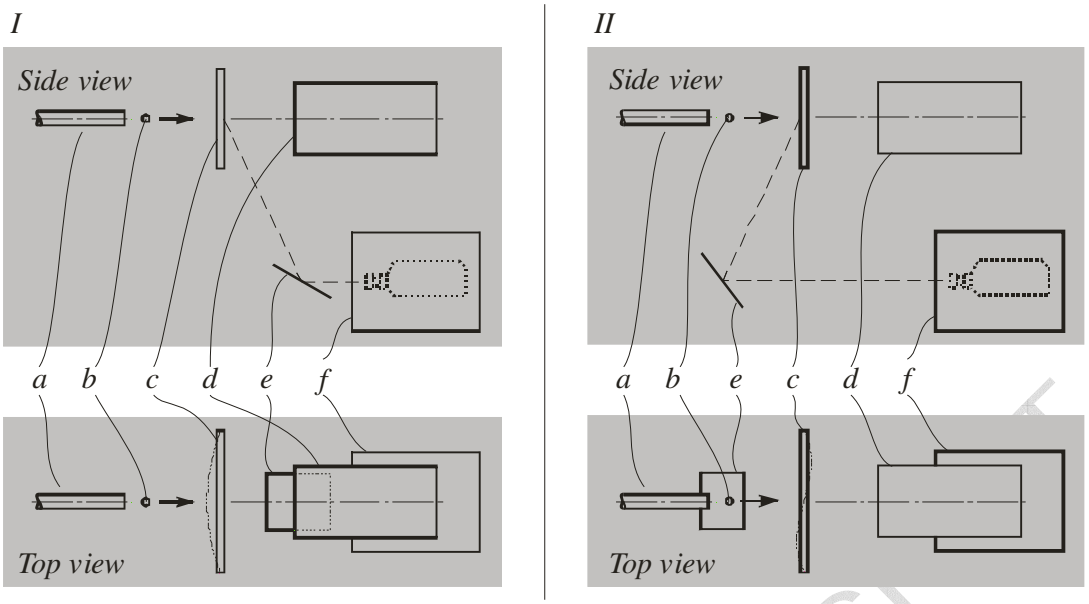

Fig. 6. Schematic of test setup for symmetric (I) and antisymmetric (II) preload. The parts are:

a: Gas gun barrel b: Impactor (10mm steel bullet) c: Test specimen

d: Bullet catcher e: Mirror f: High-speed camera in steel box

Initial tests on impact with symmetrical bending had revealed that catastrophic damage was initiated by impact-induced debonding of the back face-sheet. Consequently, the mirror was placed to permit a back side view in the symmetric preload cases. In the antisymmetric cases, the mirror was placed to permit a front side view.

A special bending rig was designed and manufactured for the purpose of these tests. Figure 7 shows the main components.

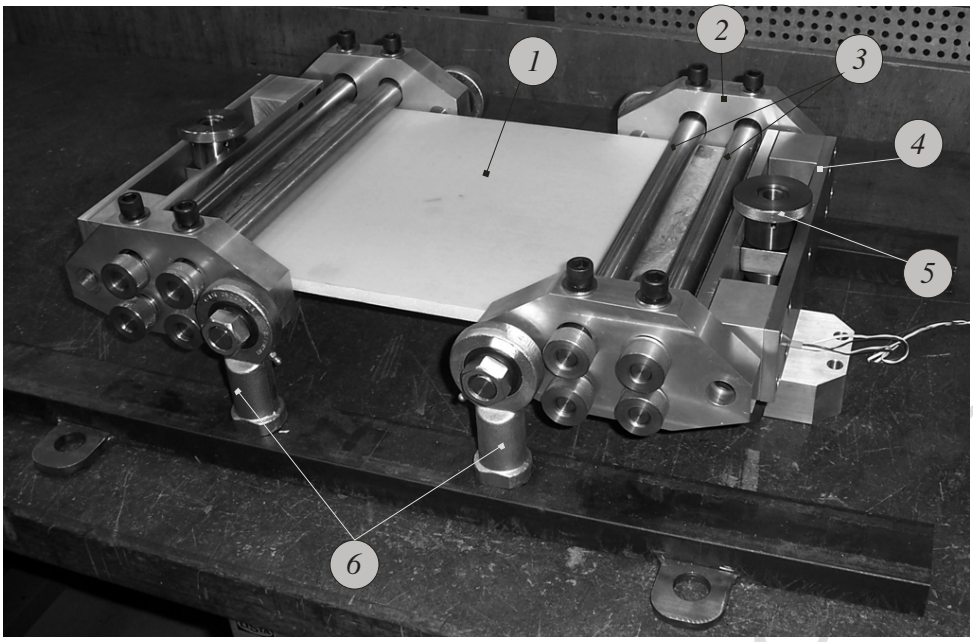

Fig. 7: Bending rig with specimen, laid out on a table for clarity. The parts are:

1: Test specimen 2: Moment yoke 3: Clamp bars

4: Load yoke 5: Load screw 6: Yoke supports

The bending rig would be bolted onto a target frame in front of the bullet catcher. A test specimen may, as shown in Figure 7, be inserted between the clamp bars (3). By rotating the load screws (5), the load yokes (4) were moved inwards or outwards, hereby acting on the moment yokes (2) and bending the test specimen. Ball-joints and edge bearings are employed to allow some freedom of deformation, as may be caused by e.g. bending-twisting coupling effects in the test specimen

5 High-speed camera recording parameters

The impact tests were recorded using an Olympus i-Speed 2 camera. The recording speed was 8000 frames/s with an exposure time of 63 μs and the frame size was 256x192 pixels. For the symmetric bending tests, the camera viewed the back side of the specimen, while for the antisymmetric tests, the front side was viewed, as indicated in figure 5. Two 650 W photo-lamps were used to obtain sufficient light for the high-

speed recordings. For better recording contrast, the specimens were painted matt white, and a 20 mm square grid was drawn using a black permanent ink marker. Furthermore, the predominantly white surface reduces heating problems caused by the photo-lamps. Even so, the photo-lamps should not be turned on more than a few seconds before shooting – a test specimen in an early test series failed due to thermal stresses induced by the photo-lamps.

6 Symmetric bending preload and impact results

With an ultimate static preload corresponding to a face sheet strain ε_{ult} = 4400 μstrain (as indicated in section 3), it was decided to set a maximum preload level corresponding to 0.6ε_{ult}. Furthermore, with only 5 test specimens available for this test scenario, it was decided to start with the maximum preload level test and decrease the preload, until no catastrophic damage occurred. The results are outlined in Table 1.

Table 1: Summary of results for symmetric bending preload and impact.

Test number	Preload strain	Catastrophic damage	Penetration
c-s-020	0.2 ε_{ult}		+
c-s-040	0.4 ε_{ult}	+	+
c-s-045	0.45 ε_{ult}	+	+
c-s-050	0.5 ε_{ult}	+	+
c-s-060	0.6 ε_{ult}	+	+

Figure 8 shows the high-speed camera recordings (first 8 frames, 0 to 0.875 μs) of test c-s-045.

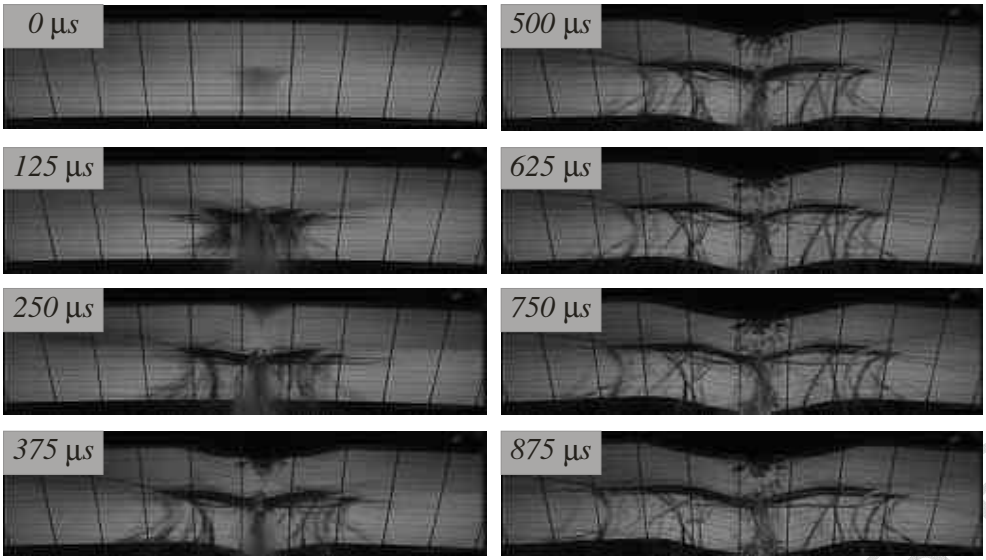

Fig. 8. High-speed camera recordings showing back side view of specimen c-s-045, from 0 to 0.875 μs.

In Figure 8, the initial frame (0 μs) shows a trace of the impactor exiting the test specimen.

At 125 μs, a plume of ejecta is seen – the intensity of the plume is reduced in subsequent frames. Also, strips of 0° fibres are peeling off to both sides of the impact point – this becomes more visible in subsequent frames. Near the impact point, a barely visible bulge indicates debonding between core and back face-sheet.

At 250 μs, the debonding bulge appears to have just reached the edge of the specimen, thus extending across the specimen width.

From 375 μs onwards, the length of the debonding bulge grows visibly, and the test specimen eventually retains negligible bending stiffness.

6.1 Failure progression analysis

The failure progression for symmetrically preloaded panels, consistent with camera recordings and subsequent post-impact analysis of the panel, is outlined in Figure 9.

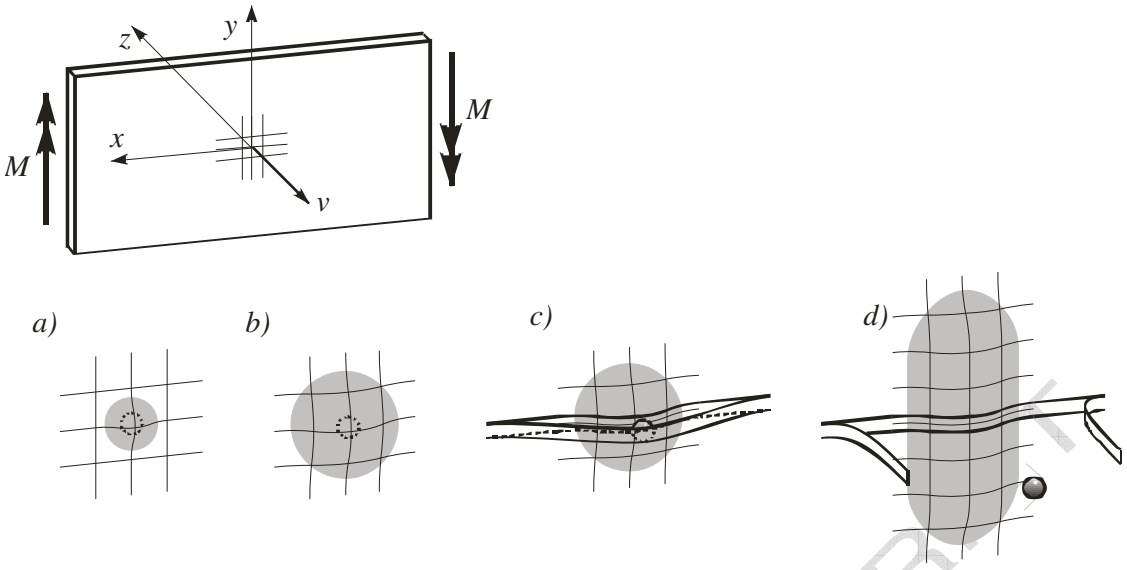

Fig. 9. Failure progression, symmetric bending. Top: Specimen, seen from the back side. v indicates the impactor velocity. a) to d): magnified view of the central area at different stages of penetration.

In Figure 9, the impactor is represented as a sphere with dashed outline (when hidden) or full outline (when exposed). Debonding is shown as grey shading. The damage progression is:

a: onset of debonding between back face-sheet and core.

b: maximum debonding size, beginning face-sheet failure

c: tearoff of central strip of outer (0°) ply

d: debonding front progressing in y-direction

When the debonding front has reached the edges, the structural capacity is governed by the bending stiffness of the face-sheets (or, more precisely, the post-buckling behavior of the compressive side face-sheet), as seen in Figure 10. The debonding distances d are given in Table 2.

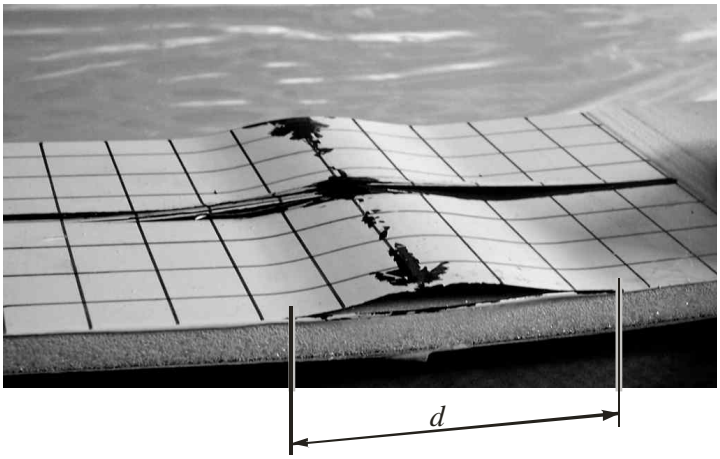

Fig. 10. Buckling of debonded compressive side face-sheet, indicating debonding distance d.

Table 2: Debonding distances d for symmetric preload tests

Specimen	c-s-020	c-s-040	c-s-045	c-s-050	c-s-060
d [mm]	n.a.	75	82	80	85

The results in Table 2 indicate an approximately constant debonding distance for the four catastrophically failed specimens.

7 Antisymmetric bending preload and impact results

The ultimate static preload corresponded to an equivalent tranverse core shear stress τ_{ult} = 1.18 MPa (as indicated in section 3). Again, 5 specimens were available, and the test series was initiated at preload level $0.6\tau_{ult}$. The results are outlined in Table 3.

Table 3: Summary of results for antisymmetric bending preload and impact.

Test number	Preload stress	Catastrophic damage	Penetration
c-a-020	0.2 τ_{ult}		+
c-a-040	0.3 τ_{ult}		+
c-a-045	0.4 τ_{ult}	+	+
c-a-050	0.5 τ_{ult}	+	+
c-a-060	0.6 τ_{ult}	+	+

Figure 11 shows the high-speed camera recordings (first 8 frames, 0 to 0.875 μs) of test c-a-060.

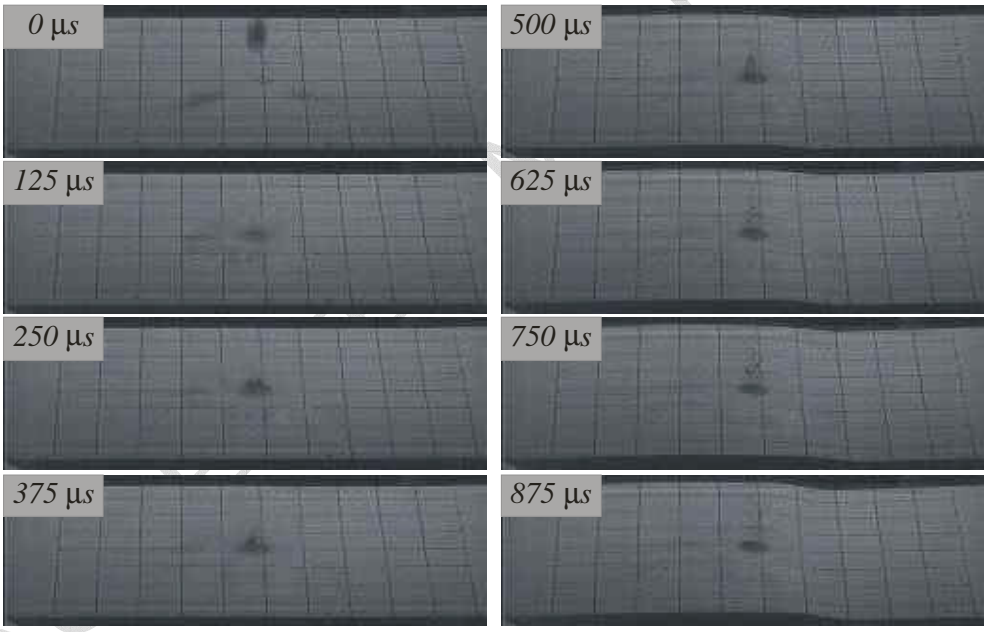

Fig. 11. High-speed camera recordings showing front side view of specimen c-a-060, from 0 to 0.875 μs.

In Figure 11, the initial frame (0 μs) shows the impactor just before hitting the test specimen. The dark spots on the specimen surface are shadow outlines of the impactor, cast by the photolamps.

At 250 μs, a rearward plume of ejecta is beginning to form – this is believed to be caused by the formation and subsequent elastic springback of a debonding bulge on the back side of the specimen.

From the images in Figure 11, it appears that shear failure occurs simultaneously across the width of the panel, initiating at about 500 μs. Closer scrutiny of the recordings reveal initiation of panel failure at about 375 μs, starting in the central part of the specimen

From 500 μs onwards, the specimen failure proceeds, as the face-sheet – core interface fails, reducing the shear carrying capacity of the panel.

7.1 Failure progression analysis

The failure progression for antisymmetrically preloaded panels, consistent with camera recordings and subsequent post-impact analysis of the panels, is outlined in Figure 12.

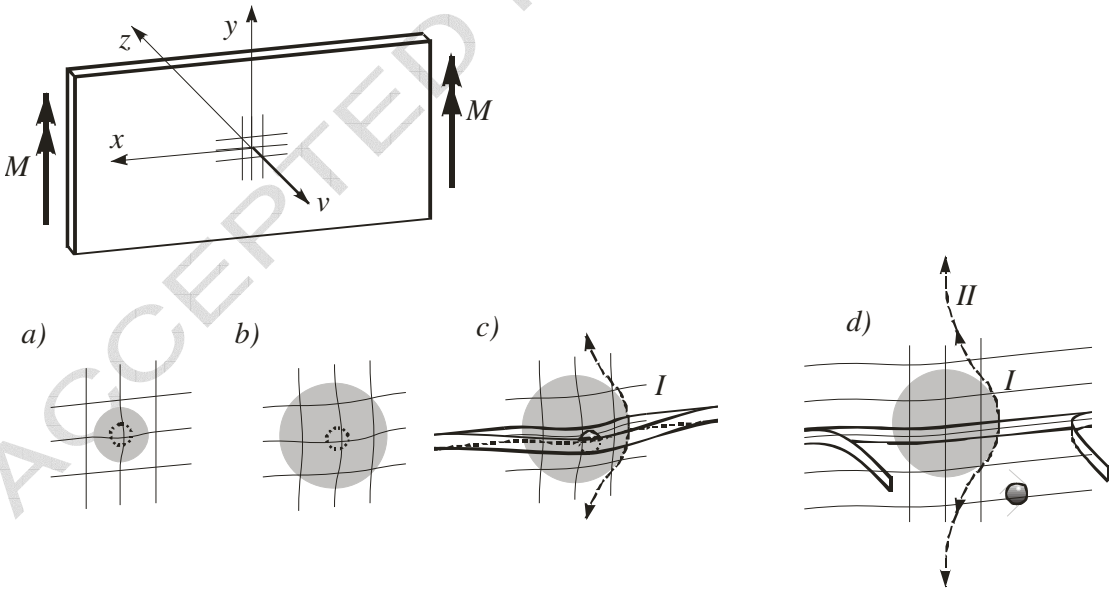

Fig. 12. Failure progression, antisymmetric bending. Top: Specimen, seen from the back side. v indicates the impactor velocity. a) to d): magnified view of the central area at different stages of penetration.

In Figure 12, the impactor is represented as a sphere with dashed outline (when hidden) or full outline (when exposed). Debonding is shown as grey shading. The damage progression is:

a: onset of debonding between back face-sheet and core.

b: maximum debonding size, beginning face-sheet failure

c: tearoff of central strip of outer (0°) ply, mode I (transverse) core fracture propagating in ± y-direction

d: Failure of central strip of outer ply, core crack kinking progressively towards shear mode failure (mode II).

A mode I transverse core crack is feasible only on the tensile-stress side of the panel, i.e. front side for positive x-coordinates and back side for negative x-coordinates, as indicated in Figure 12. The edge of the back-side debonding forms a stiffness discontinuity around the debonding, from which the transverse crack may initiate. The core cracking and direction transition from transverse to 45° is shown in Figure 13.

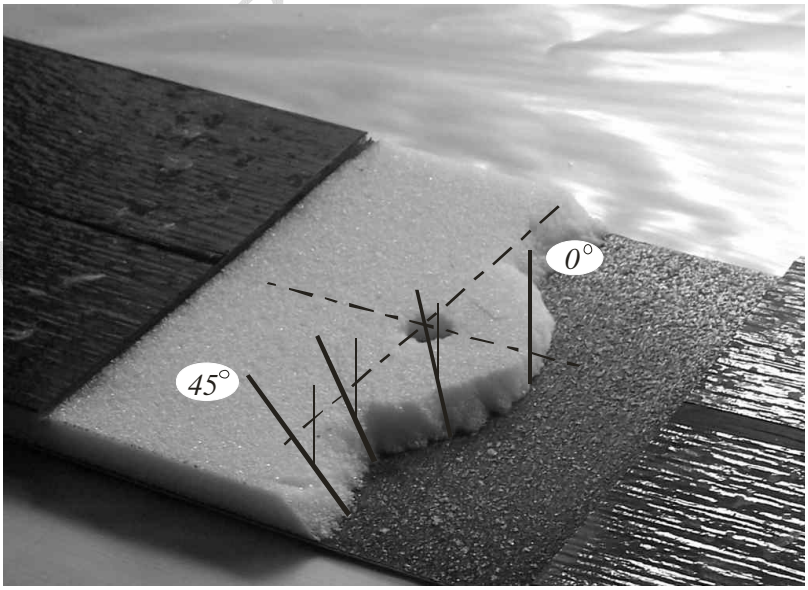

Fig. 13: Specimen c-a-060 with debonded back face sheet removed for clarity.

Eventually, the core fracture extends across the width of the specimen, whereupon the face-sheets separate from the core. The residual stiffness is, as in the case of symmetric bending, governed by the bending stiffness of the face-sheets. An edge-on view of a failed panel is shown in Figure 14. The debonding distances d are given in Table 4.

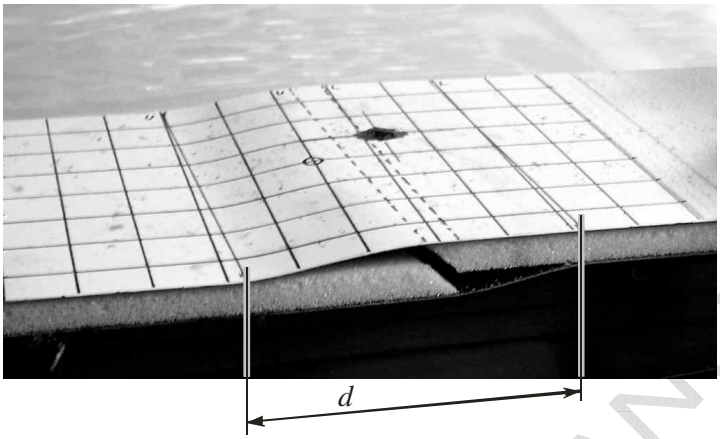

Fig. 14. Fully developed sandwich panel shear failure with extensive debonding d between core and face-sheets.

Table 4: Debonding distances d for symmetric preload tests

Specimen	c-a-020	c-a-030	c-a-040	c-a-050	c-a-060
d [mm]	n.a.	n.a.	98	130	132

The results in Table 4 indicate a moderate dependence of the debonding distance on the preload magnitude for the four catastrophically failed specimens.

8 Penetrating impact without preload

For comparison, two specimens were penetrated without preloading. The specific purpose of these tests was to verify the formation of a debonding between the back face-sheet and the core (as indicated in Figures 9 and 12). Post-impact analysis of the

specimens revealed debonds of roughly circular shape with diameters Ø of approximately 35mm and 40mm, respectively. The debond size was measured after cutting through the specimens, see Figure 15.

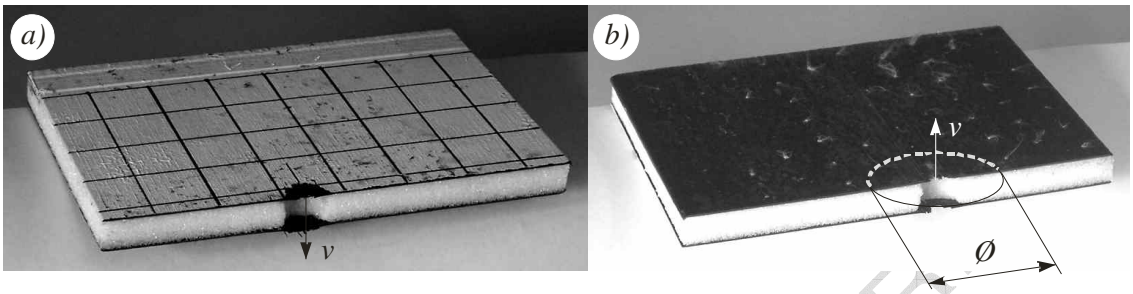

Fig. 15: Cut-through of specimen impacted without preload, as seen from the front (a) and back (b) sides. The arrows show the impactor direction. Ø indicates the size of the debond between the back face-sheet and the core.

It should be noted that the accuracy of the debond diameter measurement is approximately ± 5 mm. The core damage, as indicated in Figure 15, was restricted to punch-through removal of core material in the immediate impactor path. No cross-cracking of the core material was observed.

The damage to preloaded specimens which did not fail catastrophically was qualitatively similar to the non-preloaded specimens. The debond diameters are given in Table 5. The debond diameters are moderately larger than for the two unloaded specimens discussed above, but of similar shape.

Table 5: Debonding diameters for specimens without catastrophic damage

Specimen	c-a-020	c-a-030	c-s-020
Ø [mm]	50	50	40

9 Discussion and conclusion

The experiments described in the present paper demonstrated the possibility of catastrophic failure in a structurally preloaded sandwich panel when subjected to rapid, localized penetration. Although based on a severely limited number of experiments, the data nevertheless indicate a threshold preload level, above which the impact-induced damages will propagate. For the two preload cases treated in the present study, the threshold levels were between roughly 20 and 40% of the corresponding ultimate static load. In both cases, the onset of catastrophic failure was attributed to impact-induced debonding between the core and the back face-sheet. Post-impact analysis of unloaded control specimens and specimens loaded below the threshold level revealed a circular debonding (approximate diameter 35 – 50 mm) between the core and the back face-sheet. Since this corresponds to an equivalent reduction of the sandwich panel width, it would be instructive to repeat the experiment with panels of larger width. Likewise, variations of test parameters (impactor velocity end diameter, laminate stacking sequence, core material density etc.) have not been considered – these may well have a significant influence on the development of damage.

Constructive countermeasures against catastrophic failure should, in both load-cases, focus on increasing the strength/toughness of the interface between face-sheets and core. Post-impact analysis of the test-specimens revealed a poor interface strength, probably due to the omission of an additional adhesive film (the pre-pregs were applied directly to the foam core surface). More radical measures include peel-stoppers and through-the-thickness stitching.

In generalized terms, the cases described in this paper treat the effects of sudden, localized damage to an already prestressed structural component. This approach may be seen as the temporal reversal of classical fracture mechanics (where a locally damaged component is subjected to a structural load). It was experimentally demonstrated that the two situations share some characteristics, e.g. a threshold structural load level,

below which the local damage does not propagate, and that propagation of damage is driven by the release of elastic energy. On the other hand, the rapid penetration introduces transient dynamics which will affect the results. It is thus unlikely that similar threshold results may be reproduced by subjecting pre-damaged panels to a structural load.

10 Acknowledgments

The work presented was supported by:

The Innovation Consortium "Integrated Design and Processing of Lightweight Composite and Sandwich Structures" (abbreviated "Komposand"), funded by the Danish Ministry of Science, Technology and Innovation and the industrial partners Composhield A/S, DIAB ApS (DIAB Group), Fiberline Composites A/S, LM Glasfiber A/S and Vestas Wind Systems A/S.

US Navy, Office of Naval Research (ONR), Grant/Award No. N000140710227: "Influence of Local Effects in Sandwich Structures under General Loading Conditions & Ballistic Impact on Advanced Composite and Sandwich Structures". The ONR program manager was Dr. Yapa Rajapakse.

The support received is gratefully acknowledged

References

[1] Rosenberg, Z., Mironi, J., Cohen, A. and Levy, P., On the Catastrophic Failure of High-pressure Vessels by Projectile Impact. International Journal of Impact Engineering, Vol. 15 p. 827-831, 1994.

[2] Lu, G. Y., Zhang, S. Y., Lei, J. P. and Yang, J. L. Dynamic Responses and Damages of Water-filled Pre-pressurized Metal Tube Impacted by Mass. International Journal of Impact Engineeing, Vol. 34 p. 1594-1601, 2006.

[3] Mizukawa, K., Fujii, T., Itama, K., Osaka, K., Impact Strength of Thin-Walled Composite Structures Under Combined Bending and Torsion, Composite Structures, Vol. 4 p. 179-192, 1985

[4] Sun, C. T. and Chen, J. K., On the Impact of Initially Stressed Composite Laminates, Journal of Composite Materials, Vol. 19 No. 6, p. 490 – 504, 1985

[5] Zhang, X., Davies, G. A. O., Hitchings, D., Impact Damage with Compressive Preload and Post-Impact Compression of Carbon Composite Plates, International Journal of Impact Engineering, Vol. 22 p. 485 - 509, 1999

[6] Malekzadeh, K., Khalili, M. R. and Mittal, R. K., Response of In-plane Linearly Prestressed Composite Sandwich Panels with Transversely Flexible Core to Low-velocity Impact. Journal of Sandwich Structures and Materials, Vol.8 p. 157-181, 2006.

[7] Mitrevski, T., Marshall, I. H., Thomson, R. S. and Jones, R., Low Velocity Impacts on Preloaded GFRP Specimens with Various Impactor Shapes. Composite Structures, Vol. 76 p. 209-217, 2006.

[8] Herszberg, I. and Weller, T., Impact Damage Resistance of Buckled Carbon/Epoxy Panels. Composite Structures, Vol. 73 p. 130-137, 2006